Biophysical Journal
Article

Biophysical Society

The contribution of electrostatics to hydrogen exchange in the unfolded protein state

Rupashree Dass,[1] Enrico Corlianò,[2] and Frans A. A. Mulder[1,*]
[1]Department of Chemistry and Interdisciplinary Nanoscience Center, Aarhus University, Aarhus, Denmark and [2]Department of Chemistry, University of Florence, Sesto Fiorentino, Italy

ABSTRACT Although electrostatics have long been recognized to play an important role in hydrogen exchange (HX) with solvent, the quantitative assessment of its magnitude in the unfolded state has hitherto been lacking. This limits the utility of HX as a quantitative method to study protein stability, folding, and dynamics. Using the intrinsically disordered human protein α-synuclein as a proxy for the unfolded state, we show that a hybrid mean-field approach can effectively compute the electrostatic potential at all backbone amide positions along the chain. From the electrochemical potential, a fourfold reduction in hydroxide concentration near the protein backbone is predicted for the C-terminal domain, a prognosis that is in direct agreement with experimentally derived protection factors from NMR spectroscopy. Thus, impeded HX for the C-terminal region of α-synuclein is not the result of intramolecular hydrogen bonding and/or structure formation.

SIGNIFICANCE Hydrogen exchange (HX) is an important technique in protein science and plays an important role in studies of protein stability and folding. Unfortunately, electrostatic effects complicate the interpretation of HX rates, although the magnitude of this effect has hitherto not been accounted for. It is shown how hybrid mean-field calculations can compute the electrostatic potential along the protein chain. The associated change in the electrochemical potential then foretells the reduction in HX rates. Accounting for these effects can aid the correct interpretation of experimental HX protection factors.

INTRODUCTION

Hydrogen exchange (HX) substitution was among the earliest characterization methods to demonstrate the globular nature of proteins (1) and has been instrumental in demonstrating the presence of partial protein unfolding and the existence of a hierarchy of protein states between the unfolded and folded states of proteins and for the determination of the local stability of protein structure to unfolding (2–4). Typically, HX measurements follow the rate at which labile backbone amide hydrogens (protium, ^{1}H) exchange with deuterium (^{2}H) upon dissolution into D_2O. Alternatively, HX can be probed by transfer of magnetization saturation from the water in NMR experiments such as CLEANEX-PM (5). Chemically, the rate of exchange depends on various factors, including burial, hydrogen-bond formation, amino acid sequence composition, and external variables (such as pressure, temperature, and ionic strength) (6,7). Protein structure and hydrogen-bond formation will act to slow HX, and this deceleration is routinely expressed by "protection factors" (PFs); the PF is defined as the ratio of the "intrinsic" exchange rate, k_{intr}, in the fully unprotected, solvent-accessible state to the observed rate, k_{obs}. Reduced HX rates may also arise from other mechanisms, including inductive effects from neighboring side chains (8,9), long-range electrostatic interactions (10), and the local distribution of charged residues (11). For example, amide HX rates are very sensitive to the amino acid sequence (9), and these (mainly inductive) effects are due to the stereoelectronic properties of side chains to the left and right side of the amide group. Because "intrinsic," sequence-specific reference exchange rates for the protein sequence under consideration are typically not available, intrinsic amide HX rates are computed by proxy from data tabulated for host peptides, such as poly-D,L-alanine (8). "Intrinsic" exchange rates are thus straightforwardly, but only approximately, predicted from the primary structure by consideration of the identity of the side chains bracketing

Submitted February 24, 2021, and accepted for publication August 3, 2021.
*Correspondence: fmulder@chem.au.dk
Editor: Bernd Reif.
https://doi.org/10.1016/j.bpj.2021.08.003

each of the amide hydrogens in the sequence using a lookup table. PFs have a simple interpretation; for example, PF = 4 means that the amide proton is protected PF/(1 + PF) = 80% of the time. Therefore, HX is an attractive method to study the local structural stability in proteins, including the presence of structural motifs or domains in disordered regions (12–14).

However, to date, a quantitative description of the influence of electrostatics on HX in the unfolded state has been lacking, and this continues to limit the precision of PFs and their meaningful interpretation. In this article, we compute the electric potential along the unfolded protein chain from sequence using a mean-field approach. As a proxy for the unfolded state, we used human α-synuclein, an intrinsically disordered protein (IDP) of 140 amino acids, which is one of the most unfolded proteins currently characterized (15). Of interest for this work, the protein harbors three regions with very distinct charge patterning: an N-terminal domain (residues 1–61) rich in positively and negatively charged amino acids and with a small net positive charge, a central region (residues 62–95; also known as the nonamyloid-β component region) that is devoid of charged amino acids with two exceptions, and a highly acidic C-terminal tail (residues 96–140). Using the electrochemical potential, the concentration reduction of catalytic hydroxide concentration near the polyamide backbone was calculated to be fourfold and shown to match with experimental observation.

MATERIALS AND METHODS

Sample preparation

For HX measurements, 10 mg ^{13}C-^{15}N-labeled α-synuclein (Giotto Biotech, Sesto Fiorentino, Italy) was dissolved in 550 μL 25 mM Tris buffer (pH 9), to which 50 μL D_2O and 10 μL 50 mM 4,4-dimethyl-4-silapentane-1-sulfonic acid were added. To probe the effect of local electrostatic potential, we have used various paramagnetic co-solute probes. For co-solute paramagnetic relaxation enhancement (sPRE) measurements, two-dimensional (2D) ^{1}H-^{15}N heteronuclear single quantum coherence (HSQC) experiments were acquired. For these measurements, three samples were made, each containing 200 μM ^{13}C-^{15}N-labeled α-synuclein, 25 mM phosphate buffer (pH 7.3), and 10% D_2O. Gadoteric acid ($C_{16}H_{25}GdN_4O_8$) (sample A) or gadoteridol ($C_{17}H_{29}GdN_4O_7$) (sample B) was added to 1-mM complex concentration. Sample C (no added paramagnetic relaxation enhancement (PRE) agent) served as a diamagnetic reference.

Experimental NMR setup

Experiments were recorded on a Bruker spectrometer at ^{1}H frequency of 950 MHz equipped with a cryogenically cooled triple resonance probe. Chemical shifts were referenced with respect to 4,4-dimethyl-4-silapentane-1-sulfonic acid. Backbone assignments were taken from Biological Magnetic Resonance Data Bank (BMRB; https://bmrb.io/: 18857) and verified by conducting a three-dimensional HNCO experiment at 283 K and ^{1}H-^{15}N HSQC experiments at 283, 288, and 298 K for the sample at pH 7.52. 90° Pulse lengths were 10 μs (^{1}H), 10 μs (^{13}C), and 33 μs (^{15}N).

For determination of HX, a 2D CON experiment was adapted to include a DÉCOR module (16). The pulse sequence is available for download from www.protein-nmr.org. Experiments were performed at 298 K (pH 9). 2D data matrices consisted of 512(^{13}C) × 256(^{15}N) points (real + imaginary). The ^{15}N CPMG block was run with 2, 4, 6, 8, or 12 π-pulses in a constant time of 20 ms. The spectral widths were 3939 Hz (^{13}C) and 2310 Hz (^{15}N), respectively. Each experiment was run with eight scans, taking 5.5 h per 2D data set. A reference experiment was run at each pH and temperature, in which WALTZ-65 decoupling with RF power of 5.0 kHz was inserted on the ^{1}H channel during the CPMG period.

Gradient sensitivity-enhanced ^{1}H-^{15}N HSQC experiments were performed for measuring PRE effects at 283 K. The experiments were acquired with decoupling during acquisition and with 2048 (^{1}H) and 256 (^{15}N) time domain points. The spectral widths were 15,243 Hz (^{1}H) and 3177 Hz (^{15}N). The addition of paramagnetic complex did not cause changes in peak positions, indicating that it did not cause any change in structure or that it bound to the protein.

All NMR data were processed by NMRPipe (17) and analyzed by Sparky (18).

Determination of HX rate constants and PFs

Peak intensities of the CON spectra (extracted using Sparky) were used to calculate the rate constant using peaks for which the signal to noise ratio was larger than 5. The calculations followed published work (16,19). PFs were calculated from the relation $PF = k_{intr}/k_{obs}$, where k_{intr} was calculated from the protein sequence using the SPHERE server with default parameters (https://protocol.fccc.edu/research/labs/roder/sphere/sphere.html).

Determination of amide proton temperature coefficients

Amide proton chemical-shift temperature coefficients were calculated using published data that were recorded at 278, 288, 293, 298, and 303 K (BMRB: 18857). A value of −4.5 ppb/K demarcates the approximate border found to correspond to hydrogen-bond formation in folded proteins (20,21).

Calculation of the electrostatic potential

An equation for the energy based on analytical form (22) was used to calculate the potential as the energy divided by a unit charge, with the index i running over all the m charged residues in the protein sequence:

$$\varphi = \sum_i^m 332(6/\pi)^{(1/2)}\left[1 - \pi^{(1/2)} x exp\left(x^2\right) erfc(x)\right]/q\epsilon d, \quad (1)$$

where $x = \kappa d/6^{1/2}$, $erfc(x)$ is the complementary error function, d is the distance between charges, $\kappa = (8\pi I e^2/\epsilon k_B T)^{1/2}$ ($= I^{1/2}/3.04$ Å^{-1} at room temperature) and I is the ionic strength. d is the root mean-square distance, computed from the residue separation l as $d = bl^{1/2} + s$, where the effective bond length, b, for the Gaussian chain model was 10 Å, and the shift for the distance to the side chain, s, was set to 7.5 Å. The potential at each backbone position was evaluated using $T = 298$ K; $I = 0.025$ M. At pH 9, the charges were defined as "D": −1.0, "E": −1.0, "K": 1.0, and "R": 1.0. The N- and C-termini were neutral and charged, respectively. This calculation is equivalent to a mean-field approach. In cases in which the pH is close to the pK_a-value of one or several side chains, a self-consistent calculation can be performed following the procedures of Tamiola et al. (23).

For the analysis to take into account the effect of electrostatics on HX rates (referred to as PF*), charged residues to the left and right of the amide hydrogen under consideration were excluded from the summation.

RESULTS AND DISCUSSION

Although experimental HX rates for α-synuclein have been reported in the literature using cross-saturation (i.e., by CLEANEX-PM), we were concerned about possible artifacts stemming from cross-relaxation (24) or exchange from the hydroxyl groups of serine and threonine side chains (25). We therefore developed an alternative approach to measure HX that relies on exchange-induced incoherent dephasing of two-spin correlations (16,26), which is immune to relayed magnetization transfer artifacts. To be generally applicable to unfolded proteins and IDPs, where backbone amides may exchange so rapidly that they are not detectable at the amide hydrogen (27), we designed a proton-less 2D CON pulse sequence that employs ^{13}C detection (28) and relies on the highly favorable dispersion of backbone ^{15}N and ^{13}C′ chemical shifts in nonfolded proteins. The experiment (19) contains a CPMG (29,30) block on the ^{15}N channel, where the density operator proportional to $2C_zN_y$ is allowed to partially evolve into $4C_zN_xH_z$, generating an admixture that depends on the interpulse spacing chosen by the experimenter. Because chemical exchange will exclusively act to annihilate $4C_zN_xH_z$ by spin decorrelation (26,31), exchange-dependent signal loss will ensue. Because the method does not rely on the detection of the amide proton, we were able to detect all fast-exchanging residues of α-synuclein that otherwise disappear from HSQC spectra at high pH (25).

A series of experiments (A) was conducted by changing the number of CPMG π-pulses but keeping the total CPMG time constant to produce different admixtures of $2C_zN_y$ and $4C_zN_xH_z$. To obtain a reference signal that does not contain the exchange contribution, a second experiment (B) was conducted with WALTZ-65 decoupling on ^{1}H throughout the CPMG block. Exchange rates were determined by fitting computed ratios (A/B) to the experimentally obtained ones (16,26) using published protocols (19). The exchange rates are shown in Fig. 1 *a*. Significant variation is observed along the sequence, with a marked plunge at the C-terminus, in agreement with earlier observations (25,32,33). To account for the expected variation in intrinsic amino-acid-sequence-dependent exchange rates (9), the measured exchange rates were converted to PFs using the program SPHERE (34,35), as shown in Fig. 1 *b*. This greatly reduces the spread in the data for the region 1–100, in which PFs vary around 1 – meaning a complete lack of order. In marked contrast, the C-terminus displays values much larger than 1, which might be taken to mean that residual structure is present in the C-terminal domain (32). Because this suggestion is, however, at variance with analyses of NMR chemical shifts and scalar couplings for the C-terminus, we sought to evaluate the presence of hydrogen bonds by amide hydrogen temperature coefficients ($d\delta/dT$); in folded proteins, comprehensive analyses have shown that impeded HX due to hydrogen-bond formation is accompanied by reduced temperature coefficients such that $d\delta/dT < -4.5$ ppb/K provide strong support for H bonding (20,21). Amide hydrogen temperature coefficients were determined from deposited chemical shift for α-synuclein at several temperatures (BMRB: 18857) and are shown in Fig. 2. For the most part, values fluctuate around −6 to −7 ppb/K, typical of unstructured regions. Although possibly somewhat reduced values are seen for regions 30–50 and 120–140, these cannot explain the large PFs observed. Consequently, these data agree with a broad body of evidence that suggests an absence of persistent interactions in the monomeric protein, with only subsidiary weak electrostatic interactions existing between the N- and C-termini.

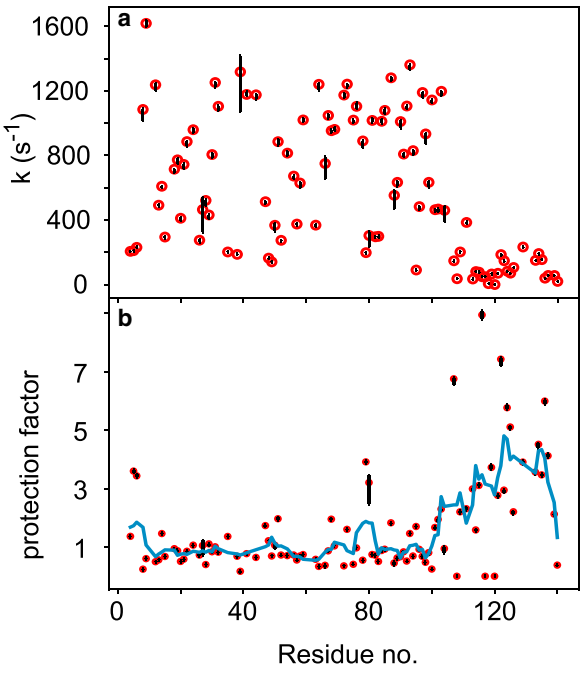

FIGURE 1 Backbone amide HX of α-synuclein. (*a*) Exchange rates with solvent at pH 9, 298 K. (*b*) HX PFs. To guide the eye, a moving average of length 5 is shown as solid line in (*b*). Error bars reflect the 68% confidence intervals (+/- one standard deviation) derived from a Monte Carlo procedure. To see this figure in color, go online.

At the same time, the preponderance of Asp and Glu residues at the C-terminus of α-synuclein will create a negative potential around the protein chain. Although the effect of the electrostatic surface potential at the protein-solvent interface on HX has been qualitatively discussed in the past (36,37), an experimental demonstration of exclusion of charged species near the backbone has hitherto been lacking. To demonstrate its reality, we compared sPRE (38,39) induced by two paramagnetic Gd(III) complexes that are physicochemically equivalent, except for their net charge: whereas gadoteric acid is negatively charged, gadoteridol is neutral. When added to the protein solution, dipolar interactions with the unpaired lanthanide

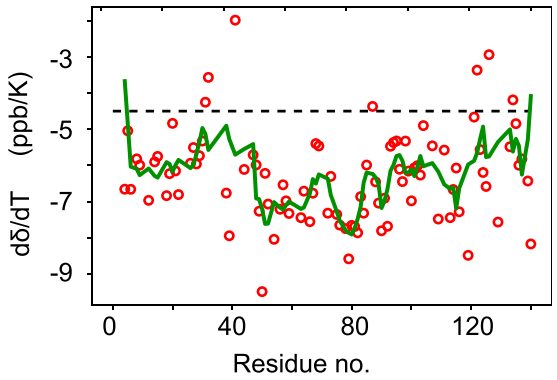

FIGURE 2 NMR chemical-shift temperature coefficients for the amide hydrogens of α-synuclein. To guide the eye, a moving average of length 5 is shown as solid line. To see this figure in color, go online.

electrons (S = 7/2) increases the relaxation rates of the protein nuclei with a $1/r^6$ distance dependence, which causes broadening of resonances for nuclei in close proximity. We compared changes in peak broadening for solutions with neutral and negatively charged co-solute, in which any region of the protein that preferentially excludes the charged ionic species will display increased intensity. Fig. 3 *a* shows the ratio of peak heights when the negative complex is added to the sample, compared with when a neutral complex is added to the sample. Whereas the neutral complex affected backbone amides more evenly, in accordance with published investigations using Ni(II) and Fe(III) complexes (40,41), the negatively charged complex caused less line broadening at the C-terminus, in accord with electrostatic repulsion.

A quantitative understanding of ion depletion can be gleaned by computing the electrostatic potential at the protein backbone. Using the Debije-Hückel approximation for a Gaussian polyelectrolyte protein chain (22,23), we computed the electrostatic potential at each amino acid in the α-synuclein backbone (Eq. 1 in Materials and methods), and the result is shown in Fig. 3 *b*. It matches very well with the observed reduction in HX, as well as with the exclusion of the negatively charged PRE agent. Because hydroxide ions in solution are the species (42) that catalyze backbone amide HX above pH 5, a lower concentration of OH^- in the vicinity of the polypeptide chain would result in a concomitant reduction in exchange kinetics, in agreement with the observations made for gadoteric acid.

In thermodynamic terms, to maintain a constant electrochemical potential at the polypeptide backbone at equilibrium, the electrostatic interaction energy acts to lower the local hydroxide concentration (43):

$$\overline{\mu} = \mu^0 + RTln(\gamma x) + zF\varphi \qquad (2)$$

Here, μ^0 is the chemical potential of the pure substance in the standard state (i.e., at reference absolute temperature T and pressure p, in which all interactions have been extinguished), R is the universal gas constant, γ is the activity constant, x is the mole fraction of ions (the activity $a = \gamma x$), z is the charge on the ion, F is the Faraday constant, and φ is the electric potential. Thus, it is possible from Eq. 2 to use the computed potential φ to estimate the concentration change of hydroxide at the protein backbone and therewith predict PFs. Identifying that the PF is proportional to the fold-change in hydroxide concentration, rearrangement of Eq. 2 gives:

$$PF = exp(-[zF\Delta\varphi/RT]) \qquad (3)$$

Thus, from the calculated electric potential, a quantitative prediction of the retardation effect on base-catalyzed HX can be made. These computed PFs for α-synuclein are shown in Fig. 3 *c*, and the trend is in good agreement with

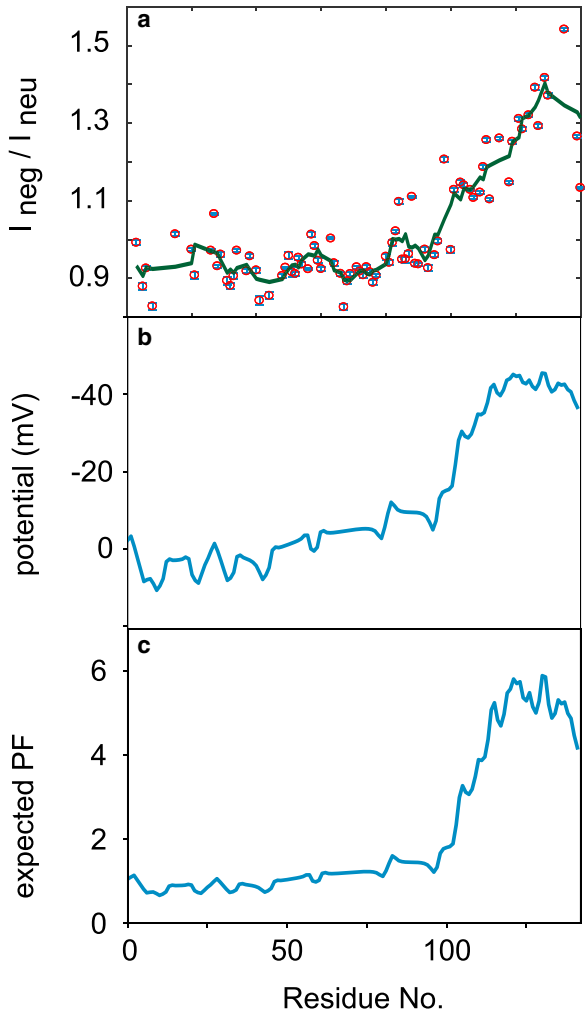

FIGURE 3 Correspondence between (*a*) reduced access to negatively charged paramagnetic chelate, (*b*) calculated electrostatic potential, and (*c*) predicted PFs for α-synuclein. To guide the eye, a moving average of length 5 is shown as solid line in (*a*). Error bars in the top panel are derived from the r.m.s. noise level in the 2D spectra. To see this figure in color, go online.

the experimental data (Fig. 1 *b*). The scatter that is observed in the experimentally derived PFs is wholly a consequence of shortcomings in the modeling of the intrinsic rate constants, and suggests that there is considerable room for improvement in the modeling of intrinsic HX rates for polypeptides.

For example, k_{intr} readily takes into account the presence of a charge at the directly flanking positions because these are an integral part of the short peptides that are used to determine them but do not consider all the remaining long-range interactions. Therefore, for a fair comparison the potential (Eq. 1) needs to be recomputed while excluding the directly neighboring charges. Dividing the experimental PFs by these electrostatic retardation factors then yields corrected factors PF* from which the electrostatic contribution is correctly removed. Any PF* significantly above 1 would then signal structure formation. Taking the PFs reported in Fig. 4 *b* of Okazaki et al. and the ones measured in this study (Fig. 1 *b*), we obtain Fig. 4. In both cases, the electrostatic correction removes the apparent protection in the C-domain. With few exceptions, the PF*s fluctuate close to 1, although there are several residues at the N-terminus that show sizable protection in the CLEANEX-PM study. Whether this points to structure formation upon going from pH 9, low salt to pH 7, or high salt or is due to shortcomings in either of the two experimental approaches remains to be clarified.

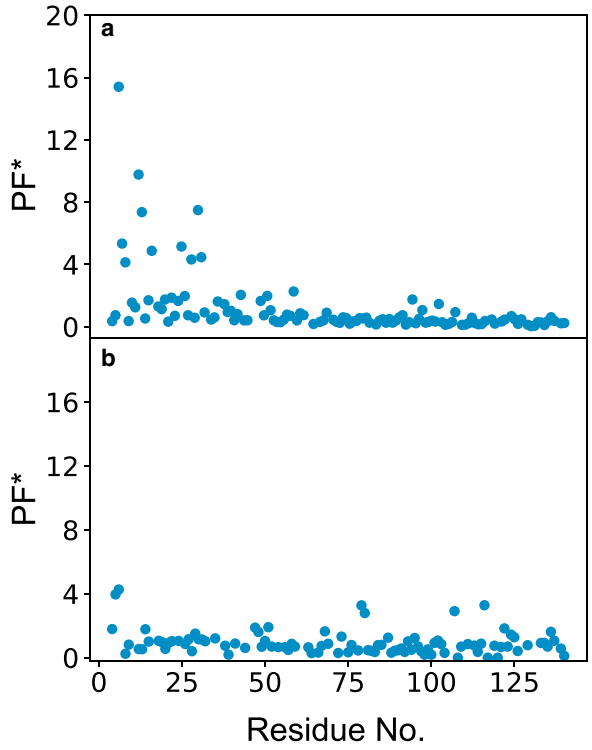

FIGURE 4 Corrected HX PFs PF* for α-synuclein. (*a*) PF* derived from curve fitting of CLEANEX-PM data obtained in the range pH 6.5–8.0, 100 mM NaCl. (*b*) PF* derived from CON-DÉCOR at pH 9, 25 mM NaCl. To see this figure in color, go online.

Although the model for calculating the electrostatics is approximate, the agreement attained here is at a level that is similar to predictions of pK_a constants in unfolded polypeptides (22,23). The observed correspondence is therefore highly encouraging and should allow more realistic ensemble-based calculations to be tested in the future.

In an early study, Alexandrescu and co-workers demonstrated (25) that amide hydrogens exchanged rapidly with solvent, confirming the unfolded nature of α-synuclein. They also explained why NMR signals were lost in in-cell ^{15}N-^{1}H HSQC spectra of α-synuclein upon raising the temperature and pH, providing a first demonstration of the persistence of its disordered state in vivo (44,45). Using CLEANEX-PM HX (5), they noticed that the C-terminal region exchanged slower than the rest of the protein and sought this explanation in the possibility that the large number of polar side chains (Thr and Ser in particular) would lead to enhanced exchange for the N-terminus relative to the C-terminal region. They also tested whether electrostatics might play a role by the addition of 300 mM sodium chloride (NaCl) and found this to 1) enhance exchange rates and 2) erase the difference in rates between the N- and C-termini. A "change in the effective pH in the vicinity to the protein compared with bulk solution" and "screening the protein from the reactive H_3O^+ and OH^- ions that catalyze exchange" were suggested as two possible explanations, but neither hypothesis was tested in their work. At a minimum, structural differences of the protein between the two conditions could be excluded as an explanation because the addition of salt did not induce chemical-shift changes. Subsequently, Okazaki et al. performed a more extensive study of HX for α-synuclein at 100 mM NaCl by CLEANEX-PM, recording data at various pH-values and experimental mixing times (32). They consistently found slower exchange in the C-terminal region at all pH-values studied. When converting their data to PFs, a pattern emerged with values around 1 (indicating full solvent exposure) for the region 30–100, whereas relatively scattered values were obtained for the N-terminus. Interestingly, in agreement with the Croke study (25), increased PFs were obtained for the C-terminal domain. Although PFs are expected to exhibit some scatter because of the limited accuracy of computed intrinsic rates from the lookup tables (25,46), the pervasive increase observed for the C-terminus was well reproduced in the two studies. Although Okazaki et al. acknowledged that exchange may be hindered by the presence of negative charge, they concluded that interaction between the N- and C-termini is the dominant factor for retardation (32). The existence of long-range interactions has also been suggested by PRE studies (47,48) using the introduction of spin labels at cysteine residues. Although misincorporation (49) of Cys at position 136 may have potentially compromised these studies by leading to

unintentional signal loss in the C-terminus, weak electrostatic interaction between the N- and C-termini are supported by other data (50,51) and have been suggested to persist in the cellular milieu (44). At the same time, monomeric α-synuclein is intrinsically disordered along its entire sequence at the local level, as judged from NMR chemical shifts (15) and scalar couplings (52). As it stands, a cogent explanation that encompasses both the lack of structure formation of α-synuclein as well as impeded HX for the C-terminus was lacking.

The combination of electrostatic modeling of the unfolded state, coupled to computation of the change in electrochemical potential, now shows that the paradox is resolved by a quantitative consideration of repulsion of catalytic hydroxide ions by acidic protein side chains. The fact that electrostatics due to local amino acid biases can have such significant effects on intrinsic HX rates has significant implications for the structural and energetic interpretation of PFs. As observed in this study, even for an IDP that is qualified as 97% disordered (15), intrinsic exchange rates calculated from the Bai-Englander tables display a wide variation, and computed PFs range from 0.1 to 10. The concurrent investigation of amide hydrogen chemical-shift temperature coefficients shows that even this large variation cannot be used to infer a dependable level of protection due to hydrogen bonding. A possible avenue to link protection to structure formation in IDPs involves the systematic investigation of protein mutations that locally change helicity; because point mutations only modify a single side chain, relative changes in HX can be accurately connected to structural propensity differences because, with exception of the mutated residue, the need for intrinsic reference rates is side-stepped in a direct comparison.

As one of the main application areas of PFs is the computation of residue-specific stabilities to unfolding, this means that $\Delta\Delta$G-values in protein stability studies from NMR- or MS-based HX are in error by 1.7 kJ/mol for every factor two that intrinsic rates are over- or underestimated. What is more, for regions of relatively high charge density–and in particular for studies performed at low ionic strength–rates in the unfolded form will show large, systematically skewed values that would lead to sizable deviations. The lack of better, more appropriate models for (locally) disordered, exchange-competent states that are operational in HX clearly limits the interpretation accuracy of stability data. By the same token, moderate variations of $\Delta\Delta$G-values observed for structural elements do not necessarily mean that they do not unfold cooperatively.

A comprehensive model for computing intrinsic exchange rates of polypeptide amide backbone hydrogens that can account for electrostatic effects offers exciting prospects to utilize HX measurements as quantitative proxies for determining the electrostatic potential around IDPs. Such methodologies would also be valuable for studies of protein liquid-liquid phase separation, where electrostatics play a key role in the formation of coacervates (53,54). Studies along these lines are in progress in our laboratory.

CONCLUSION

It is shown here that the concentration of anions in the vicinity of an acidic disordered (unfolded) protein is reduced in a way that accurately mirrors the electrostatic potential. This quantity was efficiently calculated and predicted the fourfold increase in protection from HX that was observed in experiment. These results demonstrate that a local drop in the hydroxide concentration at the protein backbone amide is the single dominant factor to explain the reduced HX rates for the C-terminal region of α-synuclein. In other words, impeded HX at the acidic tail of human α-synuclein is a direct experimental manifestation of the electrochemical potential.

SUPPORTING MATERIAL

Supporting material can be found online at https://doi.org/10.1016/j.bpj.2021.08.003.

AUTHOR CONTRIBUTIONS

R.D. performed all experiments and computations, analyzed the data, and wrote and edited the article. E.C. analyzed the data. F.A.A.M. conceptualized the study, designed the experiments and computational framework, and wrote and edited the article.

ACKNOWLEDGMENTS

We thank an anonymous reviewer for providing insightful comments to improve our manuscript and Dr. C. Nishimura (Teikyo Heisei University, Japan) for providing the PFs published in (32).

Access to the NMR spectrometers at the Danish Center for Ultrahigh-Field NMR Spectroscopy (Ministry of Higher Education and Science grant AU- 2010-612-181) is gratefully acknowledged.

REFERENCES

1. Hvidt, A., and K. Linderstrøm-Lang. 1954. Exchange of hydrogen atoms in insulin with deuterium atoms in aqueous solutions. *Biochim. Biophys. Acta.* 14:574–575.
2. Bai, Y., T. R. Sosnick, …, S. W. Englander. 1995. Protein folding intermediates: native-state hydrogen exchange. *Science.* 269:192–197.
3. Englander, S. W., and L. Mayne. 2017. The case for defined protein folding pathways. *Proc. Natl. Acad. Sci. USA.* 114:8253–8258.
4. Xue, M., T. Wakamoto, …, F. A. A. Mulder. 2019. How internal cavities destabilize a protein. *Proc. Natl. Acad. Sci. USA.* 116:21031–21036.
5. Hwang, T. L., P. C. van Zijl, and S. Mori. 1998. Accurate quantitation of water-amide proton exchange rates using the phase-modulated CLEAN chemical EXchange (CLEANEX-PM) approach with a Fast-HSQC (FHSQC) detection scheme. *J. Biomol. NMR.* 11:221–226.
6. Hernández, G., and D. M. LeMaster. 2009. NMR analysis of native-state protein conformational flexibility by hydrogen exchange. *In*

Protein Structure, Stability, and Interactions, Methods in Molecular Biology (Methods and Protocols). J. Shriver, ed. Humana Press, pp. 285–310.

7. Hvidt, A., and S. O. Nielsen. 1966. Hydrogen exchange in proteins. *Adv. Protein Chem.* 21:287–386.
8. Bai, Y., J. S. Milne, …, S. W. Englander. 1993. Primary structure effects on peptide group hydrogen exchange. *Proteins.* 17:75–86.
9. Molday, R. S., S. W. Englander, and R. G. Kallen. 1972. Primary structure effects on peptide group hydrogen exchange. *Biochemistry.* 11:150–158.
10. Kim, P. S., and R. L. Baldwin. 1982. Influence of charge on the rate of amide proton exchange. *Biochemistry.* 21:1–5.
11. Wu, K.-P., D. S. Weinstock, …, J. Baum. 2009. Structural reorganization of alpha-synuclein at low pH observed by NMR and REMD simulations. *J. Mol. Biol.* 391:784–796.
12. Hodge, E. A., M. A. Benhaim, and K. K. Lee. 2020. Bridging protein structure, dynamics, and function using hydrogen/deuterium-exchange mass spectrometry. *Protein Sci.* 29:843–855.
13. Englander, S. W., and L. Mayne. 1992. Protein folding studied using hydrogen-exchange labeling and two-dimensional NMR. *Annu. Rev. Biophys. Biomol. Struct.* 21:243–265.
14. Englander, S. W., L. Mayne, …, W. Hu. 2016. Protein folding-how and why: by hydrogen exchange, fragment separation, and mass spectrometry. *Annu. Rev. Biophys.* 45:135–152.
15. Nielsen, J. T., and F. A. A. Mulder. 2016. There is diversity in disorder-"In all chaos there is a cosmos, in all disorder a secret order". *Front. Mol. Biosci.* 3:4.
16. Dass, R., E. Corlianò, and F. A. A. Mulder. 2019. Measurement of very fast exchange rates of individual amide protons in proteins by NMR spectroscopy. *ChemPhysChem.* 20:231–235.
17. Delaglio, F., S. Grzesiek, …, A. Bax. 1995. NMRPipe: a multidimensional spectral processing system based on UNIX pipes. *J. Biomol. NMR.* 6:277–293.
18. Goddard, T. D., and D. G. Kneller. SPARKY 3. https://www.cgl.ucsf.edu/home/sparky/.
19. Dass, R., and F. A. A. Mulder. 2020. Paris-DÉCOR: a protocol for the determination of fast protein backbone amide hydrogen exchange rates. Methods in Molecular Biology. Springer US, pp. 337–344.
20. Tomlinson, J. H., and M. P. Williamson. 2012. Amide temperature coefficients in the protein G B1 domain. *J. Biomol. NMR.* 52:57–64.
21. Cierpicki, T., and J. Otlewski. 2001. Amide proton temperature coefficients as hydrogen bond indicators in proteins. *J. Biomol. NMR.* 21:249–261.
22. Zhou, H.-X. 2002. A Gaussian-chain model for treating residual charge-charge interactions in the unfolded state of proteins. *Proc. Natl. Acad. Sci. USA.* 99:3569–3574.
23. Tamiola, K., R. M. Scheek, …, F. A. A. Mulder. 2018. pepKalc: scalable and comprehensive calculation of electrostatic interactions in random coil polypeptides. *Bioinformatics.* 34:2053–2060.
24. Hwang, T.-L., S. Mori, …, P. C. M. Van Zijl. 1997. Application of phase-modulated CLEAN chemical EXchange spectroscopy (CLEANEX-PM) to detect water-protein proton exchange and intermolecular NOEs. *J. Am. Chem. Soc.* 119:6203–6204.
25. Croke, R. L., C. O. Sallum, …, A. T. Alexandrescu. 2008. Hydrogen exchange of monomeric α-synuclein shows unfolded structure persists at physiological temperature and is independent of molecular crowding in *Escherichia coli*. *Protein Sci.* 17:1434–1445.
26. Kateb, F., P. Pelupessy, and G. Bodenhausen. 2007. Measuring fast hydrogen exchange rates by NMR spectroscopy. *J. Magn. Reson.* 184:108–113.
27. Gil, S., T. Hošek, …, I. C. Felli. 2013. NMR spectroscopic studies of intrinsically disordered proteins at near-physiological conditions. *Angew. Chem. Int.Engl.* 52:11808–11812.
28. Bermel, W., I. Bertini, …, R. Pierattelli. 2006. 13C-detected protonless NMR spectroscopy of proteins in solution. *Prog. Nucl. Magn. Reson. Spectrosc.* 48:25–45.
29. Carr, H. Y., and E. M. Purcell. 1954. Effects of diffusion on free precession in nuclear magnetic resonance experiments. *Phys. Rev.* 94:630–638.
30. Meiboom, S., and D. Gill. 1958. Modified spin-echo method for measuring nuclear relaxation times. *Rev. Sci. Instrum.* 29:688–691.
31. Skrynnikov, N. R., and R. R. Ernst. 1999. Detection of intermolecular chemical exchange through decorrelation of two-spin order. *J. Magn. Reson.* 137:276–280.
32. Okazaki, H., Y. Ohori, …, C. Nishimura. 2013. Remaining structures at the N- and C-terminal regions of alpha-synuclein accurately elucidated by amide-proton exchange NMR with fitting. *FEBS Lett.* 587:3709–3714.
33. Pontoriero, L., M. Schiavina, …, I. C. Felli. 2020. Monitoring the interaction of α-synuclein with calcium ions through exclusively heteronuclear nuclear magnetic resonance experiments. *Angew. Chem. Int.Engl.* 59:18537–18545.
34. Roder, H., G. Wagner, and K. Wüthrich. 1985. Individual amide proton exchange rates in thermally unfolded basic pancreatic trypsin inhibitor. *Biochemistry.* 24:7407–7411.
35. Zhang, Y.-Z. 1995. Protein and peptide structure and interactions studied by hydrogen exchange and NMR. Dissertation. University of Pennsylvania.
36. Delepierre, M., C. M. Dobson, …, R. E. Wedin. 1987. Electrostatic effects and hydrogen exchange behaviour in proteins. The pH dependence of exchange rates in lysozyme. *J. Mol. Biol.* 197:111–130.
37. Tüchsen, E., and C. Woodward. 1985. Hydrogen kinetics of peptide amide protons at the bovine pancreatic trypsin inhibitor protein-solvent interface. *J. Mol. Biol.* 185:405–419.
38. Clore, G. M., and J. Iwahara. 2009. Theory, practice, and applications of paramagnetic relaxation enhancement for the characterization of transient low-population states of biological macromolecules and their complexes. *Chem. Rev.* 109:4108–4139.
39. Madl, T., and F. A. A. Mulder. 2018. Small paramagnetic co-solute molecules. New Developments in NMR. Royal Society of Chemistry, pp. 283–309.
40. Oktaviani, N. A., M. W. Risør, …, F. A. A. Mulder. 2015. Optimized co-solute paramagnetic relaxation enhancement for the rapid NMR analysis of a highly fibrillogenic peptide. *J. Biomol. NMR.* 62:129–142.
41. Theillet, F. X., A. Binolfi, …, P. Selenko. 2011. Paramagnetic relaxation enhancement to improve sensitivity of fast NMR methods: application to intrinsically disordered proteins. *J. Biomol. NMR.* 51:487–495.
42. Maity, H., W. K. Lim, …, S. W. Englander. 2003. Protein hydrogen exchange mechanism: local fluctuations. *Protein Sci.* 12:153–160.
43. Alberty, R. 1987. Physical Chemistry, Seventh Edition. John Wiley & Sons, New York, pp. 245–275.
44. Theillet, F.-X., A. Binolfi, …, P. Selenko. 2016. Structural disorder of monomeric α-synuclein persists in mammalian cells. *Nature.* 530:45–50.
45. McNulty, B. C., A. Tripathy, …, G. J. Pielak. 2006. Temperature-induced reversible conformational change in the first 100 residues of α-synuclein. *Protein Sci.* 15:602–608.
46. Bai, Y., J. S. Milne, …, L. Maine. 1994. Protein stability parameters measured by hydrogen exchange. *Proteins.* 20:4–14.
47. Bertoncini, C. W., Y.-S. Jung, …, M. Zweckstetter. 2005. Release of long-range tertiary interactions potentiates aggregation of natively unstructured alpha-synuclein. *Proc. Natl. Acad. Sci. USA.* 102:1430–1435.
48. Dedmon, M. M., K. Lindorff-Larsen, …, C. M. Dobson. 2005. Mapping long-range interactions in α-synuclein using spin-label NMR and ensemble molecular dynamics simulations. *J. Am. Chem. Soc.* 127:476–477.

49. Masuda, M., N. Dohmae, …, M. Hasegawa. 2006. Cysteine misincorporation in bacterially expressed human α-synuclein. *FEBS Lett.* 580:1775–1779.

50. Yoshimura, Y., M. A. Holmberg, …, F. A. A. Mulder. 2017. MOAG-4 promotes the aggregation of α-synuclein by competing with self-protective electrostatic interactions. *J. Biol. Chem.* 292:8269–8278.

51. Bernadó, P., C. W. Bertoncini, …, M. Blackledge. 2005. Defining long-range order and local disorder in native α-synuclein using residual dipolar couplings. *J. Am. Chem. Soc.* 127:17968–17969.

52. Lee, J. H., F. Li, …, A. Bax. 2015. Quantitative residue-specific protein backbone torsion angle dynamics from concerted measurement of 3J couplings. *J. Am. Chem. Soc.* 137:1432–1435.

53. Pak, C. W., M. Kosno, …, M. K. Rosen. 2016. Sequence determinants of intracellular phase separation by complex coacervation of a disordered protein. *Mol. Cell.* 63:72–85.

54. Boyko, S., X. Qi, …, W. K. Surewicz. 2019. Liquid-liquid phase separation of tau protein: the crucial role of electrostatic interactions. *J. Biol. Chem.* 294:11054–11059.